Experimental evidence for the *K-LM* radiative Auger effect in medium-mass atoms

Ch. Herren and J.-Cl. Dousse

Physics Department, University of Fribourg, CH-1700 Fribourg, Switzerland

(Received 21 May 1997)

High-resolution measurements of the $K\alpha_{1,2}$ low-energy satellites were performed for the elements $_{42}$Mo, $_{44}$Ru, $_{46}$Pd, $_{48}$Cd, and $_{50}$Sn. The photoinduced x-ray spectra were measured using a high-resolution transmission-type bent-crystal spectrometer in modified DuMond slit geometry. Experimental evidence for the *K-LM* radiative Auger effect (RAE) in solid medium-mass atoms was found and particular groups of the *K-LM* RAE transitions were identified. The experimental intensity ratios $I(K\text{-}LM$ RAE$)$ / $I(K\alpha_{1,2})$ as well as the relative intensity of the $K\text{-}L_3M_{4,5}$ transition group were extracted from the measured spectra. A comparison of the experimental results with relativistic Hartree-Fock theoretical predictions from Scofield shows a good agreement. The experimental energies of the *K-LM* RAE edges are compared with calculated Auger transition energies. [S1050-2947(97)08710-6]

PACS number(s): 32.30.Rj, 32.70.Fw, 32.80.Hd, 32.80.Dz

I. INTRODUCTION

If one creates an inner-shell hole in an atom, by x-ray or charged particle bombardment, the vacancy state decays by the well known radiative transition process (fluorescence) or the nonradiative Auger effect (electron emission). In fact, these two decay channels represent the most often observed decays of an excited atom, and the ratio of radiative to nonradiative deexcitation is given by the fluorescence yield. However, another alternative decay channel is possible, called the radiative Auger effect (RAE). In this decay process an x ray and an electron are simultaneously emitted [1], and the transition energy is shared between the two ejectiles. The RAE transitions can in general be identified easily due to their characteristic line shape. As the energy is shared between the electron and the photon, the RAE x-ray energy is given by

$$h\nu = E(K\text{-}L_iM_j) - E_{\text{kin}}(M_j), \qquad (1)$$

where the first term represents the energy of the Auger electron, and the second the kinetic energy of the M_j electron. The kinetic energy of the ejected electron can take values from zero to $E(K\text{-}L_iM_j)$. Consequently, the energy of the emitted photons corresponds to a continuous distribution, with a maximum value of $E(K\text{-}L_iM_j)$ when the kinetic energy of the electron is zero; this maximum energy appears in the spectrum as a sharp onset smeared out by the instrumental resolution. It has been shown that in radiative Auger (RA) transitions most electrons are ejected with very small kinetic energies [2], so that the largest intensity of a RA transition is observed at the onset energy. This means that for a solid target most of the electrons excited into the continuum by a RA transition lie just above the Fermi surface. Thus the spectrum of a RA x-ray fluorescence line is characterized by an onset on the high-energy side, and a long tail of decreasing amplitude on the low-energy side. Consequently, the RA x-ray emission results in a satellite structure on the low-energy tail of the diagram lines. As other processes than RA can contribute to the low-energy-tail structure of the diagram lines, RA spectroscopy at energies of some keV requires high-resolving instruments with a resolution of the order of few eV. To our knowledge, there are by now no theoretical predictions for the line shape of the photon continuum emission.

The RAE is thus a sort of intermediate decay between purely radiative and purely nonradiative deexcitation. This alternative deexcitation mode for a vacancy was predicted by Bloch and co-workers [3,4], and was first observed for dipole electric transitions by Åberg and Utriainen [5]. The study of the radiative Auger effect is currently of interest both theoretically and from the point of view of applications, as it can provide important information on the many-particle interaction of atomic systems. For a precise analysis of proton-induced x-ray emission (PIXE) data a good knowledge of the RAE intensity is of great importance. In fact, it has been shown recently [6] that the RAE, satellite, and hypersatellite yields can significantly influence the tabulated x-ray emission rates. The consideration of these competitive decay channels can improve the accuracy of trace element concentrations in the high-resolution PIXE method. In addition, a more precise knowledge of the RAE line shapes would be very helpful in x-ray photoelectron spectroscopy [7–9], x-ray fluorescence or x-ray line-shape measurements. On the other hand, the RAE in medium-mass elements also represents an interesting subject for theoreticians, as the theory is particularly challenging at higher Z, where relativistic effects have to be included.

As the radiative Auger effect is a quite weak process, experimental data are rarely found in literature. Especially for the *K-LM* RAE, experimental data are very scarce and the inconsistencies between existing experimental values and theoretical predictions are considerable. Although different theoretical approaches exist, as the shake model, the configuration interaction [10], or the radiative field calculations [11], no satisfactory agreement with the experimental data was obtained for low-Z elements, all theoretical models overestimating significantly the measured RA yields. It also has to be mentioned that complete and detailed calculations have been done only for a few elements, as for example Ar [12]. In contrast to that, we have shown recently [13] that experimental intensity ratios of the *K-MM* RAE are in quite good

agreement with theoretical predictions for elements with atomic numbers $42 \leqslant Z \leqslant 50$. It was thus a particular aim of the present study to verify if the *K-LM* RAE yields of the same mid-*Z* elements are also well predicted by theory. To date, most *K-LM* RAE measurements were carried out for low-*Z* elements or for noble gases, where solid-state and molecular structure effects can be neglected. High-resolution measurements of the *K-LM* RAE were only performed for Ca and Ti [14] and for the noble gases Kr and Xe [15]. Other available quantitative measurements were carried out with semiconductor detectors, which have poor resolution as compared to crystal spectrometers. It is therefore not astonishing that these measurements are not very accurate. In addition, the *K-LM* RA transitions lie close in energy to the $K\alpha_{1,2}$ lines (a distance of some 100 eV), so that reliable results can only be obtained with high-resolving instruments.

To the authors' knowledge, there are no other published experimental data concerning the *K-LM* RAE in elements with $42 \leqslant Z \leqslant 50$. The principal aim of this study is thus to extend the available database of the *K-LM* radiative Auger intensities to higher-*Z* elements. A second objective is to compare the observed RA edge energies to semiempirical Auger transition energies [16].

II. EXPERIMENT

A. Experimental setup

The target x-ray emission was induced by irradiating the samples with the bremsstrahlung of a commercial 3-kW x-ray tube. The tube was equipped with a gold anticathode and operated at 80 kV $\times$ 30 mA. The energy domains corresponding to the *K-LM* RAE spectra and the parent $K\alpha_{1,2}$ diagram lines were observed with a high-resolution transmission-type bent-crystal spectrometer. Complementary measurements, which will be described in detail in Sec. II B, allowed us to determine the contribution of the background, diagram line tails, and parasitic transitions to the intensity observed in the RAE regions. The *K-LM* RAE yields were then determined by subtracting these contributions from the raw spectra.

The bent-crystal spectrometer employed in this work was described in detail in the already mentioned recent publication on the *K-MM* radiative Auger effect (see Ref. [13], and references therein). As the instrumental setup for the present study was very similar, only features specific to the *K-LM* RAE measurements will be presented below.

The main change in the instrumental setup concerns the crystal. As the *K-LM* RAE yields are approximately ten times weaker than the *K-MM* ones, a thinner crystal plate (0.5 mm thick instead of 1 mm) was chosen. The gain in the spectrometer luminosity resulting from the diminution of the x-ray absorption in the crystal was increased between 1.2 and 1.7, depending on the photon energy, i.e., on the measured target. The new crystal had the same orientation as the one used in the *K-MM* measurements [(110) reflecting planes normal to the plate surface]. It was bent cylindrically to a nominal radius of 315 cm. The best angular resolution was, however, obtained for an effective radius of curvature of 311.6 cm. The spectrometer was operated in the modified DuMond slit geometry. For the chosen 0.15-mm slit width the instrumental response was found to be 10.5 arcsec, which

corresponded to energy resolutions varying from 5.7 to 11.8 eV for the average energy of the *K-LM* RAE domains of Mo and Sn, respectively. The same targets as the ones used in the *K-MM* experiment were employed, i.e., metallic foils of Mo (54.0 mg/cm^2), Pd (56.5 mg/cm^2), Cd (45.4 mg/cm^2), Sn (40.2 mg/cm^2), and Ru powder ($45\mu \leqslant$ particle size $\leqslant 400$ μ) glued on an Al backing.

For the registration of the diffracted x rays, the Phoswich scintillation detector presented in Ref. [13] was again employed. The precision in the determination of the extremely weak *K-LM* RA yields being strongly dependent on the background fluctuations, it was of prime importance in our measurements to keep the noise level at the smallest possible value. In this respect, the Phoswich detector which allowed us to suppress most of the Compton events originating from high-energy photons was very helpful.

B. Method of measurements

All measurements were performed in first order of reflection. As the intensity of *K-LM* RA transitions is extremely low for mid-*Z* elements, very long measuring times were needed for each target. In order to reduce the effect of long-term variations in the x-ray tube intensity on the RA yields, the *K-LM* RAE spectra were measured in several successive step-by-step scans. Each individual scan contained about 150 points with a step width of 4–6 eV. The measuring time was 300 sec per point. As about 24 scans were performed for each element, the total acquisition time was about 2 h per point or about two weeks per target. Between each scan, the strong $K\alpha_{1,2}$ diagram lines were briefly measured to survey the reproducibility of the instrument and the stability of the x-ray tube intensity. The aim of these $K\alpha_{1,2}$ measurements was to normalize *a posteriori* the intensity and the energy of the different scans. As all RAE spectra were measured in the direction of decreasing energy, a diminution of the x-ray tube intensity would have resulted in a systematically higher count rate on the high-energy side of the spectra. No significant change in the intensity nor in the energy of the $K\alpha_{1,2}$ lines was found, however. The largest energy shift observed for the $K\alpha_1$ centroid was about 0.3 eV. Concerning the $K\alpha_1$ intensity fluctuations, they were found to be of about 0.3%, and no systematic decrease of the intensity was observed. Therefore, no correction was performed, and for each target the total RAE spectrum was built up by summing all scans off-line. For illustration, Fig. 1 shows the total spectrum corresponding to the palladium target. After each scan the background was measured just below the region of interest. The sum of these background scans allowed us to determine the background which had to be subtracted from the measured *K-LM* region. Shorter measurements were also performed on the other side of reflection to look for possible instrumental asymmetries. As the same line shape was obtained on both sides of reflection, no asymmetries of this type were taken into account. The energy calibration of the RAE spectra was performed by measuring the $K\alpha_1$ line in first order on both sides of reflection, and using the $K\alpha_1$ line energy quoted by Bearden [17]. As mentioned above, a precise knowledge of the background shape was needed for a correct determination of the RAE yields. In our experiment the main part of the background originated from the coherent scatter-
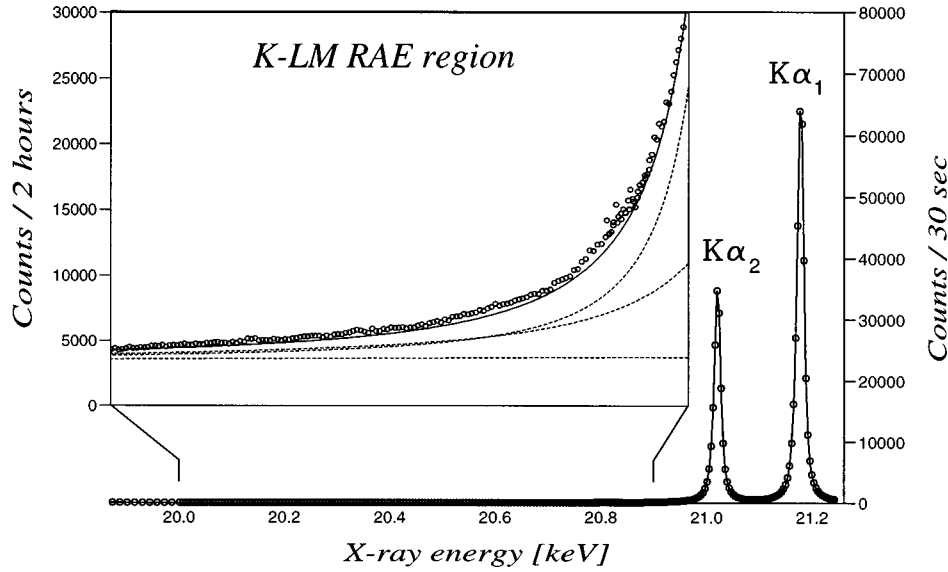
FIG. 1. Palladium $K\alpha_{1,2}$ spectrum with an enlarged view of the tail in the inset. The axis labels on the right side correspond to the $K\alpha_{1,2}$ diagram spectrum, the one on the left to the enlarged RA tail spectrum. The dotted lines in the inset show the fitted background and tails of the diagram lines, whereas the solid line represents their sum. The small difference between this sum and the measured points corresponds to the radiative Auger effect $K\text{-}LM$. The RAE residual spectra are presented for all investigated elements in Figs. 2(a)–2(e).

ing by the targets of the radiation emitted by the x-ray tube. For this reason, the angular domains corresponding to the K-LM RAE energy regions of the different elements were re-measured, replacing the target by the x-ray tube anode itself. Assuming that the coherent scattering cross sections are almost constant over the 1-keV-wide scanned energy domains, the shape of the background could be precisely determined from these measurements which in the following are called ''x-ray tube anode measurements''. A linear dependence on the energy was found for the background corresponding to the five targets (see Fig. 3). The observed slopes of the background arise from the spectral intensity distribution of the x-ray tube, and to a smaller extent from the energy dependence of the crystal reflectivity and crystal absorption. In addition, the x-ray tube anode measurements revealed the presence of weak parasite x-ray lines in the energy regions of interest. The intensities of these lines were determined relative to the background, and then subtracted from the RAE spectra.

III. DATA ANALYSIS

All spectra were analyzed by means of a least-squares-fitting procedure (package MINUIT [18], CERN Library PACKLIB) using Voigt profiles for the diagram lines. The Voigt profiles $V(E)$ were obtained by convoluting the Gaussian instrumental response of the spectrometer $G(E)$ with the Lorentzian natural line shape of the transition line $L(E)$,

$$V(E) = \lim_{n \to \infty} \int_{-n}^{+n} L(E - E') G(E') dE'$$

$$= \lim_{n \to \infty} \int_{-n}^{+n} \frac{A}{(\frac{1}{2}\Gamma)^2 + (E - E' - E_o)^2}$$

$$\times \exp(-(E')^2/2\sigma^2) dE', \qquad (2)$$

where A gives the peak amplitude, E_0 the energy of its centroid, Γ the Lorentzian full width at half maximum, and σ the standard deviation of the Gaussian distribution. The function $V(E)$ was evaluated numerically by means of the complex error function method [19,20]. The analysis of each spectrum was carried out in three consecutive steps.

(i) We first fitted the x-ray tube anode measurements, using linear functions and, where needed, Voigt profiles for the parasite x-ray lines. In fact, in the spectra of Mo, Cd, and Sn such lines were found and, except for Mo, identified. They are represented for illustration in Figs. 3(a)–3(c), and will be discussed in Sec. IV A. For the Ru and the Pd target no parasitic lines were observed, and only the linear functions were determined. As mentioned in Sec. II B, each RAE scan was followed by a background measurement in which a ten-point-wide interval located below the RAE region was scanned. The sum of these background scans allowed us to determine the average background amplitude below the RAE region. Ascribing this amplitude to the energy corresponding to the center of the interval, and using the slope obtained from the corresponding x-ray tube anode measurement, we were able to determine for each target the straight line describing the backgrounds pertaining to the RA and diagram line spectra. Actually, in order to appraise the influence of the background level on the RAE yields, for each target the analysis was carried out twice, once employing an upper limit background and once a lower limit background. The two backgrounds were given the same slope, but the standard deviation of the measured background was either added to the mean value of the latter (upper limit) or subtracted from it (lower limit).

(ii) The $K\alpha_{1,2}$ diagram lines were then analyzed using one Voigt profile for each transition and the linear functions obtained in the preceding step of the analysis for the backgrounds. The intensities of the diagram lines and the Gaussian instrumental width were let free in the fitting procedure whereas the natural Lorentzian widths of the lines were kept
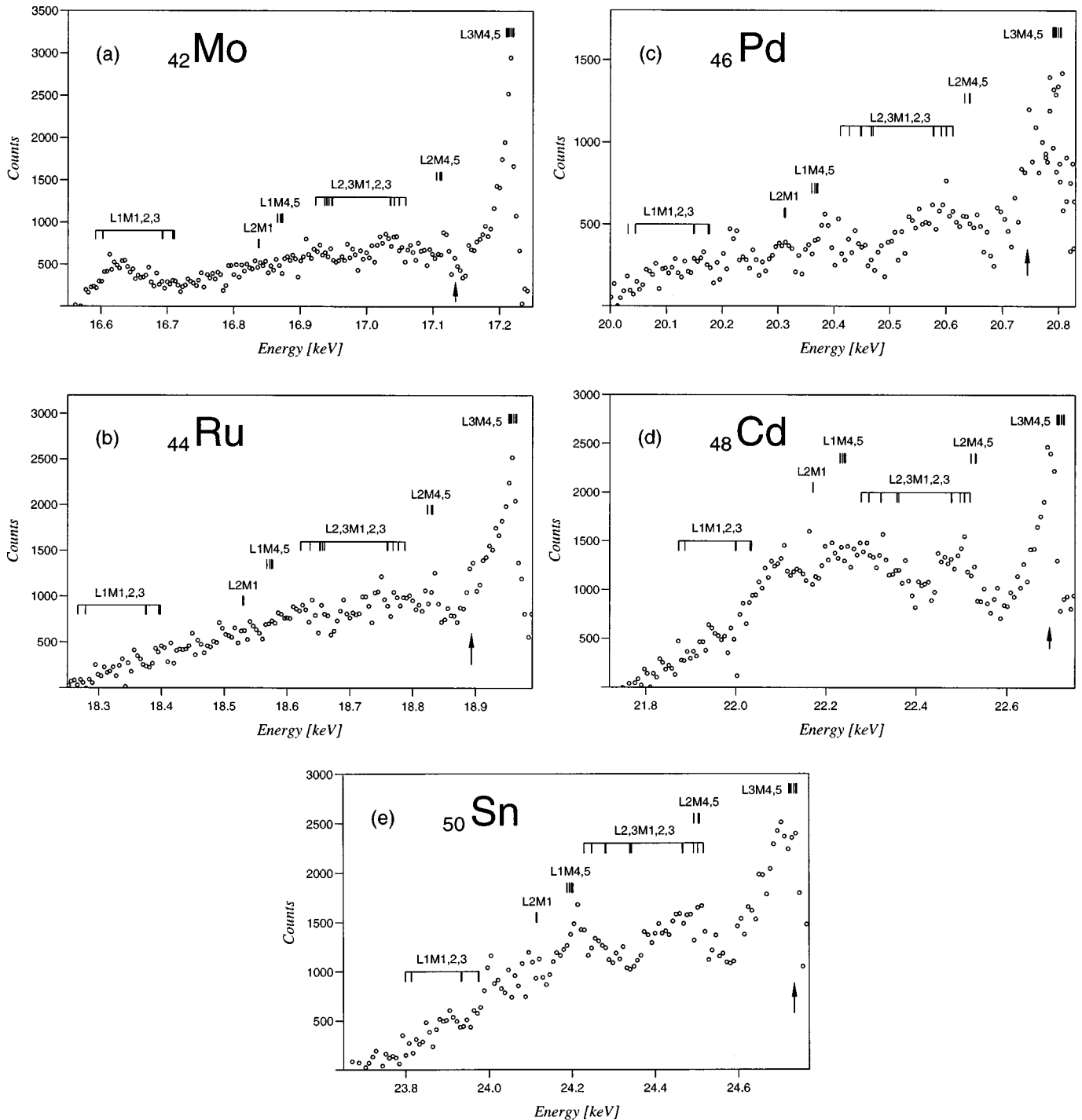
FIG. 2. *K-LM* RAE residual spectra of the investigated targets were obtained by subtracting the sum of the background and diagram line contributions from the measured spectra (this procedure is described in Sec. III and is illustrated in Fig. 1). Each spectrum is normalized to a measuring time of 2 h per point. The small bars indicate the positions of semiempirical Auger electron energies taken from Ref. [16]. The arrows indicate the energy of the dipole-forbidden $K\alpha_3$ transition, which is discussed in the text.

fixed at the values quoted by Salem and Lee [21]. The energy regions containing visible RA structures were not considered in this stage of the analysis. The intensity ratios $I(K\alpha_2):I(K\alpha_1)$ obtained from the fits were used to check the accuracy of the analysis. As shown in Table I, all ratios were found to agree with Scofield's theoretical predictions [22], with some reservation for Mo for which a 2% smaller value was obtained. The contribution of the $K\alpha_{1,2}$ tails and

background to the yields observed in the *K-LM* RAE region of Pd is shown in Fig. 1.

(iii) The fitted low-energy tails of the diagram lines, and the linear functions corresponding to the upper and lower limits of the background were then subtracted from the sum of the RAE scans, which resulted for each target element in two residual spectra reflecting the lower and upper limits of the *K-LM* RAE yields. As these residual spectra presented
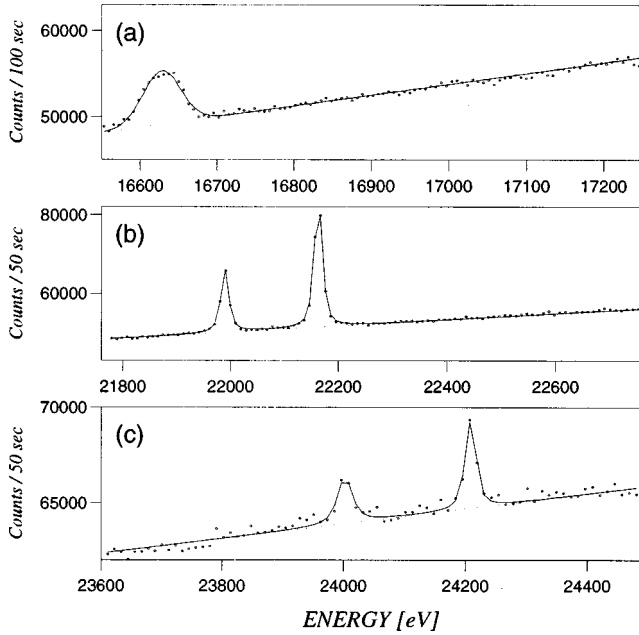
FIG. 3. ''X-ray tube anode measurements'' of the elements (a) Mo, (b) Cd, and (c) Sn showing the linear increase of the background as a function of energy as well as parasite x rays which were identified as follows: (a) unknown, (b) the $K\alpha_{1,2}$ x-rays of $_{47}$Ag, and (c) the $K\alpha_{1,2}$ x-rays of $_{49}$In. For the two other investigated elements Pd and Ru a linear function with no parasite x-ray lines was found.

complex structures, the RAE yields were determined by the numerical integration method of Simpson. The average values between the so-obtained lower and upper limits of the RAE yields divided by the fitted $K\alpha_{1,2}$ diagram line intensities are presented in Table II. The quoted errors correspond to the half-differences between the two RAE yield limits. For illustration, Fig. 2 shows the resulting residual spectra after subtraction of the measured background and of the fitted $K\alpha_{1,2}$ diagram lines.

IV. RESULTS AND DISCUSSION

A. Processes influencing the *K-LM* intensity

1. Processes competitive with K-LM RAE

As the RAE spectra cover a wide domain, it cannot be excluded *a priori* that other processes contribute to the structure observed on the low-energy tail of the $K\alpha_{1,2}$ diagram

TABLE I. Comparison of the experimental intensity ratios $I(K\alpha_2)/I(K\alpha_1)$ found in this experiment with theoretical predictions taken from Scofield [22].

Element	Ratio $\dfrac{I(K\alpha_2)}{I(K\alpha_1)}$	
	Experiment	Theory
$_{42}$Mo	0.514 ± 0.005	0.525
$_{44}$Ru	0.530 ± 0.005	0.527
$_{46}$Pd	0.528 ± 0.005	0.529
$_{48}$Cd	0.527 ± 0.005	0.532
$_{50}$Sn	0.538 ± 0.004	0.535

TABLE II. Experimental ratios for *K-LM* RAE relative to $K\alpha_{1,2}$. The theoretical values were interpolated from the predictions given by Scofield's RHF theory [11]. These ratios and other values obtained for lower-*Z* elements as well as the corresponding theoretical predictions are also plotted vs the atomic number of the targets in Fig. 4.

Element	Ratio $\dfrac{I(K-LMRAE)}{I(K\alpha_{1,2})}$	
	Experiment (in %)	Theory (in %)
$_{42}$Mo	0.087 ± 0.014	0.109
$_{44}$Ru	0.088 ± 0.013	0.095
$_{46}$Pd	0.074 ± 0.019	0.086
$_{48}$Cd	0.074 ± 0.011	0.079
$_{50}$Sn	0.075 ± 0.010	0.075

lines. Since in addition RAE intensities are very weak, such competitive processes, if not considered, may lead to systematic errors in the determination of the RAE yields. Thus a careful investigation of the possible contributing processes was done. In the previous paper dealing with the *K-MM* RAE [13], we already discussed some of these processes. We have shown in particular that Raman scattering [23] as well as radiative electron rearrangement [24] are negligibly weak for mid-*Z* targets and the experimental setup used. In addition, in that study, we also proved experimentally that solid-state or molecular effects are too weak to influence the RAE structure in a significant way. These findings also apply to the present work, and will thus not be repeated here. Furthermore, *K-LM* RAE transitions to higher bound states (shake-up transitions), which are characterized by symmetric line profiles and are hence easily recognizable, were not observed. This is, however, not surprising for medium-mass elements because shake-up to shake-off yield ratios decrease rapidly with growing values of the atomic number *Z*. Regarding this point, it has to be mentioned that our previous *K-MM* study did not reveal any RA shake-up structure either. Another possible source of systematic errors resides in the fact that the five investigated elements are characterized by filled or partly occupied $4s$, $4p$, and $4d$ levels. Hence it is possible that the observed residual intensities attributed to the *K-LM* RA effect are partially due to *K-LN* transitions. Theoretical predictions indicate that the total *K-LN* RA intensity is approximately 1.7 times smaller than the *K-LM* one [11]. Furthermore, the largest contributions are expected from the transitions in which $N_{4,5}$ electrons are involved. These transitions, however, do not influence the *K-LM* yields because they lie higher in energy. As we did not find anywhere the *K-LN* RAE edge energies, nor the corresponding Auger electron energies the following crude approximation was employed:

$$E(K-L_iN_j) \approx E(K-L_i) - E_{\text{bind}}(N_j), \quad (3)$$

where $E(K-L_i)$ is the energy of the diagram line, $E_{\text{bind}}(N_j)$ is the binding energy of the ejected electron, and i and j stand for the concerned subshells. Using this estimation, one finds that only the $K-L_1N_j$ RA transitions may overlap with the *K-LM* ones. The edges of the $K-L_2N_j$ RA lie indeed at

least 100 eV (for Mo) above the investigated regions and their influence on the measured K-LM intensity is thus probably negligible. The same holds for the K-L_3N_j RA transitions which are expected to appear between the $K\alpha_1$ and $K\alpha_2$ diagram lines, i.e., at much higher energies than the observed spectra. In general, radiative transitions which are forbidden by the selection rules contribute only poorly to the RA structure. K-L_1M_j (this paper) and K-M_1M_j [13] RA transitions were indeed found to have very low intensities. It is thus highly improbable that K-L_1N_j RA transitions contribute significantly to the observed K-LM RAE yields. This statement is confirmed by the fact that no RA onset was observed at the energies where K-L_1N_j RA transitions were expected to occur.

2. Parasite x rays in the region of interest

Parasite x-ray lines lying in the measured RA energy region are easy to identify thanks to their symmetric line profile. They may originate from impurities in the x-ray tube anode, trace elements in the targets, or the x-ray emission of target chamber pieces which are irradiated by the x-ray tube and viewed by the crystal through the slit. These lines have in general a very small intensity, and are thus not expected to influence the shape of the target x-ray spectrum very much. However, when structures such as RAE of very small intensity are measured, these contributions may become significant. In the present study parasite x-ray lines were observed in the K-LM region of molybdenum, cadmium, and tin. They will be discussed in detail hereafter.

In the case of molybdenum no narrow characteristic x-ray line was observed in the residual spectrum. But, comparing the RAE spectrum of Mo with those of the other target elements (Fig. 2), we found that the molybdenum spectrum was the only one which showed an apparent strong contribution of the K-$L_1M_{1,2,3}$ RA transitions. Figure 3(a) shows, however, that this structure was also present in the x-ray tube anode measurements. No satisfactory explanation was found for this broad structure, but the observation of the latter in the measurement performed without the Mo target excludes the possibility of a RAE origin. As it was not possible to separate the parasite structure from the K-$L_1M_{1,2,3}$ RA transitions in the residual spectrum, the following method was used. First we determined the intensity of the bump from the fit of the x-ray tube anode measurements. Assuming then that the relative intensity of the unidentified bump with respect to the linear background was the same in the x-ray tube anode spectrum and in the RAE one, we were able to subtract the surplus of intensity due to the parasitic structure from the residual spectrum. The subtracted yield represented 2.1(8) % of the whole K-LM RA intensity.

In the residual spectrum of the cadmium target two narrow lines were observed at energies of 22 162(1) eV and 21 990(1) eV. Comparing these values with the transition energies quoted by Sevier [25], one found that these parasite lines corresponded to the $K\alpha_{1,2}$ diagram transitions of silver. Actually the Cd target foil contained some Ag traces, but in too small an amount ($\sim$ 7 ppm) to explain the observed intensities of the two lines. In addition, the latter were also observed in the x-ray tube anode spectrum, indicating that the Ag $K\alpha_{1,2}$ lines found in the Cd RAE spectrum had indeed a double origin: the target itself and the anode of the x-ray tube. For this reason, the method we used for the Mo target to subtract the parasite yields could not be employed. However, as in the residual spectrum the Ag lines were quite well resolved, they could be fitted and then subtracted from the RAE spectrum before integrating the latter with the Simpson method. The RAE spectrum of Cd after the subtraction of the parasitic lines is shown in Fig. 2(d). The Ag $K\alpha_{1,2}$ lines were fitted using one Voigt profile per transition, and keeping fixed the transition natural linewidths, and the $K\alpha_2/K\alpha_1$ yield ratio. For the latter a value of 0.531 was taken [22], whereas the natural linewidths were interpolated using the tables of Salem and Lee [21]. The energies, the Gaussian linewidths, and the $K\alpha_1$ intensity were, on the contrary, used as free fitting parameters.

In the x-ray tube anode measurements corresponding to the tin target [Fig. 3(c)], two parasite lines were also observed. From their energies (24 210 and 24 002 eV, respectively) they could be identified as the $K\alpha_1$ and $K\alpha_2$ diagram lines of $_{49}$In. As the target foil of Sn was certified to contain no indium traces, the origin of the contamination was attributed to the x-ray tube anode. In the residual spectrum the two indium lines could not be resolved properly from the underlying RAE structures, so that the same method as the one used for the Mo target was employed for the subtraction of the yield pertaining to the parasite transitions. The latter was found to be 2.6(4) % relative to the total K-LM RAE intensity.

Another x-ray transition that may affect the measured RAE spectra is the weak $K\alpha_3$ ($2s_{1/2} \rightarrow 1s_{1/2}$) transition. The latter is forbidden by the selection rules of the nonrelativistic electric dipole ($E1$) and electric quadrupole ($E2$) single-electron transitions. It has been shown recently that Scofield's theoretical predictions for the $K\alpha_3$ intensity [22] of elements ranging between $Z=54$ and 79 are in good agreement with experimental values [26]. In particular, no systematic deviation as a function of Z was observed between experiment and theory, over the whole target range. Using the predictions of the theoretical work of Scofield, we can estimate the contribution of the forbidden $K\alpha_3$ transition to the observed RAE intensity. The $I(K\alpha_3):I(K\alpha_{1,2})$ yield ratio is found to be 7 ppm for molybdenum, increasing up to 21 ppm in the case of tin. The percentage contribution of this line to the K-LM RAE yield is thus very small, varying between 0.8% for molybdenum up to about 2.8% for tin. Nevertheless, as Scofields' predictions [22] seem to be reliable, our RAE yields were corrected to account for the $K\alpha_3$ transitions. For illustration, we have inserted in Figs. 2(a)– 2(e) the energies of the $K\alpha_3$ transitions, which were calculated using the binding energies given by Sevier [25]. In some spectra, at theoretical energy of the $K\alpha_3$ a small bump lying on the RAE structure can be observed. For Cd and Sn, however, the $K\alpha_3$ is masked by the stronger K-$L_3M_{4,5}$ RA transitions.

B. K-LM radiative Auger effect

1. Intensity

As already described in Sec. III, the intensity of the K-LM radiative Auger effect was found by integrating the residual spectra with the integration method of Simpson. For all targets the theoretical predictions from Scofield [22] for
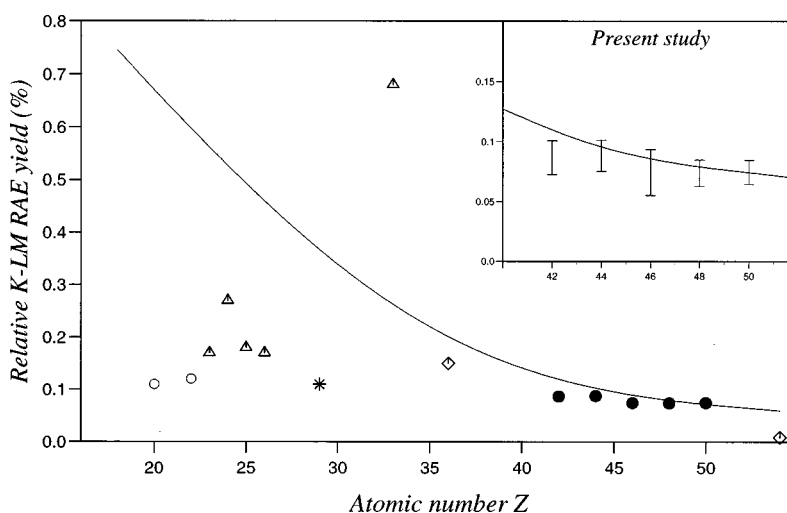
FIG. 4. Comparison of published experimental data of relative $I(K\text{-}LM)/I(K\alpha_{1,2})$ yield ratios with theory, as a function of Z. The solid line is an interpolation of theoretical values from Scofield's RHF theory [11]. ●, this work. ◇, Ref. [15]. ○, Ref. [30]. △, Ref. [31]. *, Ref. [32].

the $K\alpha_3$ intensity were subtracted from the results of the integration. In addition, the molybdenum as well as the tin RAE yields were corrected for the observed parasite x rays, as discussed above. The final results are listed in Table II. In Fig. 4 they are confronted, with other existing $K\text{-}LM$ data, to theoretical predictions from Scofield's relativistic Hartree-Fock (RHF) calculations. Scofield's calculations are the only ones which were performed for many elements throughout the Periodic Table. The errors of the intensity ratios $I(K\text{-}LM$ RAE):$I(K\alpha_{1,2})$ are not easy to determine. It is not difficult to estimate the error originating from the Simpson integration method, but this error is very small compared to other possible uncertainty sources. In fact, the largest error arises from the background, which has to be subtracted from the measured spectra. Although the standard deviations of the background fluctuations from the mean values were only of about 1%, the differences in the RAE yields obtained by subtracting the upper and lower background limits resulted in uncertainties which represent about 80% of the total errors quoted in Table II. The remaining 20% stem from the errors of the background slopes determined from the x-ray tube anode measurements, the fits of the $K\alpha_{1,2}$ spectra and from the Simpson integration method (about 3%). Errors stemming from the determination of the parasite x rays and from the $K\alpha_3$ intensity only play a minor role and were neglected.

The experimental $I(K\text{-}LM$ RAE):$I(K\alpha_{1,2})$ yield ratios obtained in previous measurements for lower-Z elements and Xe, the single heavier element for which $K\text{-}LM$ RAE results were found in the literature, are about 2–5 times weaker than predicted by theory. In contrast to that, we observe that our experimental results concerning medium-mass elements agree well with Scofield's predictions over the whole investigated region of the atomic number Z. For molybdenum a slightly smaller intensity than predicted is found. It is noteworthy to mention that theory also overestimated by the same order of magnitude the Mo $K\text{-}MM$ RAE yield [13]. On average, our intensities are slightly lower than theory. However, except for molybdenum, all obtained intensities are within the experimental errors in excellent agreement with theory. The main problem of shake calculations, which are

built on the sudden approximation model, is that they do not account for changes in the atomic potential during the RA transition. The same problem appears in Coster-Kronig transitions [27,28], where the ejected electrons are also characterized by low kinetic energies. This represents the main source of uncertainty in the available RA calculations and may be the reason for the observed large discrepancies between experimental and theoretical results in the low-Z region.

It can be seen in the residual spectra presented in Figs. 2(a)–2(e) that the RA transitions $K\text{-}L_{2,3}M_{4,5}$ represent the main contribution to the observed $K\text{-}LM$ RAE structure. This has already been found in a recent measurement of the $K\text{-}LM$ RAE in the noble gases $_{36}$Kr and $_{54}$Xe [15]. In addition, although no clear RA onset is observed, the $K\text{-}L_{2,3}M_{1,2,3}$ transitions also seem to give a significant contribution to the observed spectra. In general, the extraction of the relative intensity of particular transition groups is very difficult for different reasons. Some groups are not well resolved, or they have an intensity which is too small to be extracted with a reasonable error. The major problem, however, is the unknown shape of the individual transitions. Each transition has a long asymmetrical tail, extending down to an energy which is in principle zero. Below a certain energy it is thus very difficult to distinguish the low-energy tail of the extended RAE profile from the underlying background. The energy distribution of the photons emitted as a result of a RA shake-off transition is so broad that the low-energy part of the distribution, in spite of its very small intensity, can contribute significantly to the RA yield. This difficulty may have led to some underestimation of the $K\text{-}LM$ RAE intensity.

For each target we have estimated the intensity of the $K\text{-}L_3M_{4,5}$ RAE group which is the strongest one. The transitions pertaining to the group are quite well separated from the other RAE transitions except those of the $K\text{-}L_{2,3}M_{1,2,3}$ and $K\text{-}L_2M_{4,5}$ groups with which there is a certain overlap. The intensity was determined by fitting the $L_3M_{4,5}$ structure with several Voigt profiles. The energy region extending below the $K\text{-}L_2M_{4,5}$ edge was, however, not included in the fit,

TABLE III. Estimated contributions of the K-$L_3M_{4,5}$ RA transition group to the total K-LM intensity (lower limit values).

Element	$I(K\text{-}L_3M_{4,5})$ / $I(K\text{-}LM)$
$_{42}$Mo	0.33 ± 0.07
$_{44}$Ru	0.42 ± 0.08
$_{46}$Pd	0.35 ± 0.07
$_{48}$Cd	0.44 ± 0.09
$_{50}$Sn	0.48 ± 0.09

so that the extracted intensity corresponds to a lower limit of the K-$L_3M_{4,5}$ RAE yields.

The results of these estimations are presented in Table III. It turns out that the relative contributions of the K-$L_3M_{4,5}$ transitions represent about 40% of the whole K-LM intensity or even more if one considers that the quoted values are lower limits. Furthermore, it seems that there is some trend for the K-$L_3M_{4,5}$ contribution to increase with Z. This statement has, however, to be regarded with some reserve because the corresponding errors are quite large. The latter result mainly from the very complex and unknown tail form.

In Fig. 5 we present a summary of the K-LM and K-MM RAE data we have collected in the investigated region $42 \leqslant Z \leqslant 50$. The plot shows the ratio between our experimental values and the theoretical predictions of Scofield. The K-MM data were taken from Ref. [13]. It can be seen in this plot that for practically all investigated cases the mean intensity is slightly lower than the one predicted by theory. The single exception to these systematic lower values is found for the K-MM measurement of ruthenium. In general, however, a satisfactory to good agreement is found, and the deviations from theory, when significant, are much smaller than the ones observed in lower-Z elements and in xenon (Fig. 4).
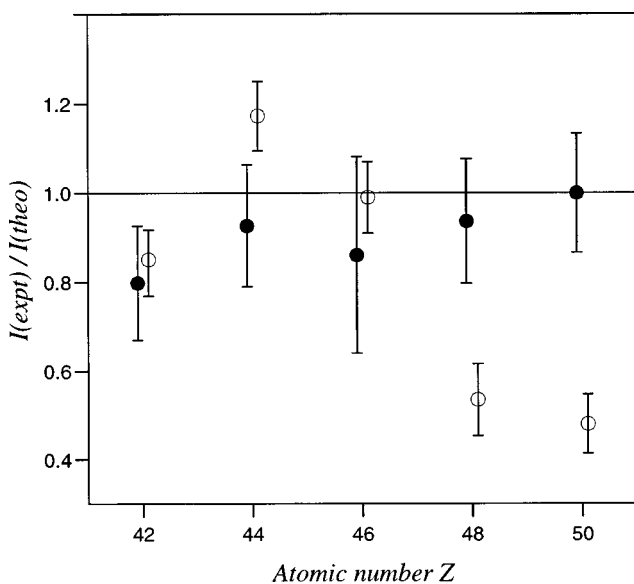
FIG. 5. Comparison of K-LM (●) and K-MM (○) RAE yield ratios with Scofield's theoretical values [11], as a function of Z. The K-MM intensities were taken from an earlier publication [13]. For clarity the K-LM and K-MM data corresponding to the same value Z were slightly shifted.

2. Edge energies

The edge energy of a RA transition, when the final state of the electron is just above the Fermi level, is identical with the Auger electron energy relative to the Fermi level, since the interaction of the outgoing electron with the hole is small. Due to the complexity of the RAE spectra, and the weak peak-to-background ratios characterizing the K-LM RAE transitions, it is almost impossible to extract the exact edge energies of the observed transition groups. Actually, as there are many possible final states which often have similar energies, abrupt edges cannot in general be observed. The fact that the edge is smeared out due to the instrumental resolution of the spectrometer does not help. It also has to be noted that the theoretical energies from Ref. [16] do not take into account relativistic and correlation effects. Thus quite important differences can result. If one compares the semiempirical line energies from Ref. [16] to calculations by Chen [29] which take into account these effects, discrepancies of about 5–25 eV are indeed found in the case of the K-MM RAE of medium-mass elements. For all these reasons, we have not extracted the RAE edge energies from the residual spectra. However, in Figs. 2(a)–2(e) we indicate the theoretical transition energies of the K-LM transitions (small vertical bars) and of the overlapping $K\alpha_3$ transition (arrow). With respect to the above-mentioned theoretical and experimental difficulties, one can state that there is generally a good agreement between the semiempirical edge energies and the observed onsets of the RA transition groups, at least for the strongest transitions, i.e., the K-$L_3M_{4,5}$. In the spectra of Mo and Ru the onsets of the K-$L_2M_{4,5}$ are observed at energies which are in quite good accordance with the semiempirical values. This statement has, however, to be considered with reserve, the presence of the close-lying $K\alpha_3$ transition making this observation a little bit doubtful. For the other target elements, the K-$L_{2,3}M_{1,2,3}$ as well as the K-$L_2M_{4,5}$ contribute significantly to the RA intensity, but no clear RA onset is observed.

V. CONCLUSION

To our knowledge the present study provides the first experimental evidence of K-LM RAE in solid medium-mass elements. The yield ratios $I(K$-LM RAE$):I(K\alpha_{1,2})$ could be determined with a precision of the order of 15% for Mo, Ru, Pd, Cd, and Sn. For each element about half of the total observed RAE intensity was found to originate from the K-$L_3M_{4,5}$ transition group. The rest of the intensity was attributed to K-L_1M_{1-5}, K-L_2M_{1-5}, and K-$L_3M_{1,2}$ transitions, which were also observed but not resolved.

Our experimental RAE yields were compared to results of Scofield's RHF calculations. The comparison shows that the agreement between theory and experiment is much better than one could expect from other measurements performed on lower-Z elements. In the atomic number region $Z \leqslant 30$, the available data indicate indeed that theory overestimates the experimental K-LM intensities by a factor of 2–6, whereas the results obtained in the present study for the region $42 \leqslant Z \leqslant 50$ are almost consistent with Scofield's predictions. In the intermediate region $31 \leqslant Z \leqslant 41$, to our knowledge, a single experimental result for the K-LM RAE exists and concerns Kr ($Z = 36$). The relative intensity found in this

work is about 30% smaller than the theoretical prediction. It thus seems that the Z dependence of the experimental RAE yields is less pronounced than predicted by Scofield's calculations. The same conclusion was drawn in our previous work devoted to the K-MM RAE, but in this case the disagreement between theory and experiment in the low-Z region was found to be less pronounced.

The edge energies of the RAE groups were compared to theoretical predictions for Auger electron energies. Considering that these theoretical values do not take into account relativistic and correlation effects, and in view of the encountered experimental difficulties, a quite satisfactory agreement was found.

As a concluding remark, we would like to point out that additional K-LM and K-MM experimental data in the atomic number region $31 \leqslant Z \leqslant 41$ could probably help to clarify the large discrepancies observed between theory and experiment in the low-Z region. In this respect, K-LL RA transitions, if observable, would also contribute to unraveling the problem. In addition, more extensive and precise calculations concerning the asymmetrical shape of the RAE shake-off transitions and the partial probabilities of the different components pertaining to the same RAE group are highly desirable. They would allow a more detailed analysis of the measured spectra and a better understanding of relaxation and multielectron processes in atomic systems.

ACKNOWLEDGMENT

---

[1] T. Åberg, in *Atomic Inner-Shell Processes*, edited by B. Crasemann (Academic Press, New York, 1975), p. 353.

[2] M. O. Krause, T. A. Carlson, and R. D. Dismukes, Phys. Rev. **170**, 37 (1968).

[3] F. Bloch and P. A. Ross, Phys. Rev. **47**, 884 (1935).

[4] F. Bloch, Phys. Rev. **48**, 187 (1935).

[5] T. Åberg and J. Utriainen, Phys. Rev. Lett. **22**, 1346 (1969).

[6] M. Budnar and A. Mühleisen, Nucl. Instrum. Methods Phys. Res. B **75**, 81 (1993).

[7] R. Manne, Chem. Phys. Lett. **5**, 125 (1970).

[8] F. Hopfgarten and R. Manne, J. Electron Spectrosc. Relat. Phenom. **2**, 13 (1973).

[9] F. R. McFeely *et al.*, Phys. Rev. B **9**, 5268 (1974).

[10] T. Åberg, Phys. Rev. A **4**, 1735 (1971).

[11] J.H. Scofield, Phys. Rev. A **9**, 1041 (1974).

[12] V. O. Kostroun and G. B. Baptista, Phys. Rev. A **14**, 363 (1976).

[13] Ch. Herren and J.-Cl. Dousse, Phys. Rev. A **53**, 717 (1996).

[14] A. Mühleisen *et al.* (unpublished).

[15] A. Mühleisen, M. Budnar, and J.-Cl. Dousse, Phys. Rev. A **54**, 3852 (1996).

[16] F. P. Larkins, At. Data Nucl. Data Tables **20**, 311 (1977).

[17] J. A. Bearden and A. F. Burr, Rev. Mod. Phys. **39**, 78 (1967).

[18] F. James and M. Ross, Comput. Phys. Commun. **10**, 343 (1975).

[19] C. J. Batty, S. D. Hoath, and B. L. Roberts, Nucl. Instrum. Methods **137**, 179 (1976).

[20] K. S. Kölbig, Commun. ACM **15**, 465 (1972).

[21] S. I. Salem and P. L. Lee, At. Data Nucl. Data Tables **18**, 235 (1976).

[22] J. H. Scofield, At. Data Nucl. Data Tables **14**, 121 (1974).

[23] T. Suzuki, J. Phys. Soc. Jpn. **22**, 1139 (1967).

[24] K. A. Jamison *et al.*, Phys. Rev. A **14**, 937 (1976).

[25] K. D. Sevier, At. Data Nucl. Data Tables **24**, 352 (1979).

[26] B. Galley and J. Cl. Dousse, Phys. Rev. A **50**, 3058 (1994).

[27] K. G. Dyall and F. P. Larkins, J. Phys. B **15**, 4103 (1982).

[28] K. R. Karim and B. Crasemann, Phys. Rev. A **31**, 709 (1985).

[29] M. H. Chen, Phys. Rev. A **31**, 177 (1985).

[30] M. Budnar *et al.*, Nucl. Instrum. Methods Phys. Res. B **63**, 377 (1992).

[31] J. L. Campbell *et al.*, Phys. Rev. A **33**, 2410 (1986).

[32] N. Maskil and M. Deutsch, Phys. Rev. A **38**, 3467 (1988).